

Photocatalytic Studies of La,Ce Co-Doped ZnO Nanoparticles

Syed Irtiqah^a and Atikur Rahman^{a,*}

^a Department of Metallurgical and Materials Engineering, National Institute of Technology Srinagar, Hazratbal, Srinagar, 190006 India

*e-mail: atikurrhmn@gmail.com, atikurrhmn@nitsri.net

Received December 14, 2019; revised December 8, 2020; accepted December 12, 2020

Abstract—Zinc oxide nanoparticles were co-doped with varying concentrations of lanthanum (La) and cerium (Ce) ions using co-precipitation method. The resulting powders were calcined in a muffle furnace for 1 h at a temperature of 500°C to produce La,Ce-doped ZnO nanoparticles of varying stoichiometry viz. ($\text{Zn}_{0.98}\text{La}_{0.01}\text{Ce}_{0.01}\text{O}$, $\text{Zn}_{0.96}\text{La}_{0.02}\text{Ce}_{0.02}\text{O}$, $\text{Zn}_{0.94}\text{La}_{0.03}\text{Ce}_{0.03}\text{O}$, and $\text{Zn}_{0.92}\text{La}_{0.04}\text{Ce}_{0.04}\text{O}$). This method of co-doping is cost effective and does not require any complex procedure, equipment or inert gases. The synthesized samples were characterized using X-ray diffraction (XRD) and scanning electron microscopy (SEM) to study the size, phases and grain morphology. XRD patterns revealed the hexagonal wurtzite phase of the synthesized samples. The average size of the undoped and La,Ce co-doped ZnO nanoparticles, as calculated from XRD pattern, was found to be 25 nm. Further, the size of co-doped nanoparticles decreased significantly with increasing dopant concentration. Optical properties were studied through UV-Visible spectrophotometry. The photocatalytic activities of undoped and La,Ce co-doped ZnO nanoparticles were examined by observing the decomposition of Rhodamine B dye under UV lamp within 0–80 min. The Rhodamine B (RB) dye solution was efficiently photo-degraded within 35 min when using $\text{Zn}_{0.92}\text{La}_{0.04}\text{Ce}_{0.04}\text{O}$ as catalyst, mechanism of which has been thoroughly discussed below. Further, photoluminescence (PL) studies revealed the narrowing of band gap with increase in concentration of dopant ions as indicated by the red shift in the PL emission spectrum of co-doped nanoparticles.

Keywords: ZnO, La and Ce co-doping, co-precipitation, photoluminescence, photocatalyst, rhodamine B, rare earths

DOI: 10.1134/S1070427220120137

INTRODUCTION

Nanoparticles have revolutionized the modern technological work because of their exuberant properties and applications in varied fields. These properties of nanoparticles pertain to their unique size, shape and surface area to volume ratio. Any change in shape and size greatly affects the properties [1, 2]. Optoelectronic properties of transition metal oxide nanoparticles have been extensively studied in the past. It has been found that rare earth doping in such nanomaterials further enhances their properties making them highly useful in optoelectronic devices [3]. Rare earth doped semiconductors have been used previously as luminescent materials in fluorescent lamps, cathode ray tubes, light emitting diodes (LEDs), solar cells

etc[4]. Recently, attention has been shifted to using luminescent materials for environmental remediation. The *n* type semiconductor, zinc oxide (ZnO), with direct band gap of 3.3 eV and a large binding energy is highly useful in optoelectronics, photocatalysis and photoluminescence [5, 6]. ZnO acts as an excellent host for rare earth ion doping that buttresses the optical properties for widespread applications in solar cells [7], light emitting diodes, photo detectors [8] and optically activated lasers [9].

Photocatalysts have wide applications in remediation of water pollution which is one of the main contributors to the environmental pollution that is threatening the existence of mankind. Photocatalysis is a promising low cost, eco-friendly and sustainable alternative for environmental remediation and energy

conservation. ZnO possesses high photosensitivity and oxidation potential making it one of the most potent UV activated photocatalysts for air and water purification [10, 11]. In addition ZnO is abundantly available, much cheaper and eco-friendly. Semiconductor based photocatalysts convert light energy into chemical energy which can later be utilized for a number of applications. So far TiO₂, ZnO, and Fe₂O₃ have been used as light sensitizers in light actuated redox reactions owing to their electronic structure which comprises of a filled valence band and an empty conduction band [12–14]. When a photon of sufficient energy more than the band gap strikes a semiconductor, electrons are pumped from valence band to conduction band leaving behind holes. Due to lack of a suitable scavenger, these electrons and holes recombine within nanoseconds and dissipate the energy as heat. However if a scavenger or surface defect site is present for electrons and holes, the recombination can be prevented and the trapped electrons and holes pave the way for redox reactions. The valence band electrons and conduction band holes hence generated, act as powerful oxidants and reductants, respectively [15, 16]. Holes have a high oxidizing power and most of the photo-degradation reactions can be attributed to this property of holes.

The photocatalytic activity of undoped ZnO with a wide bandgap (3.37 eV) is limited under UV irradiation only, i.e., $\lambda < 380$ nm, which contributes to only about 5–8% of the useful photons from sunlight while as visible light contributes to about 46% of solar energy. So to obtain a better photocatalyst from ZnO, its absorption edge needs to be from UV to visible. Furthermore the recombination rate of electron hole pairs is very high in case of undoped ZnO which also limits its utilization as photo catalyst [17, 18]. Many methods have been employed so far to overcome these limitations. However, doping with rare earth ions has resulted in considerable narrowing of band gap and better charge separation between photo-generated electrons and holes [19]. This improvement can be attributed to their distinctive *4d* and *5f* electronic configuration and special spectral characteristics. In addition, the optical band gap of ZnO can also be tailored with rare earth ion doping [20]. A number of rare earth ions of lanthanum (La) [21–23], dysporium (Dy) [24, 25], and cerium (Ce) [26] have been doped into ZnO for better photocatalytic degradation of organic pollutants.

Samarium (Sm) and neodymium (Nd) dopings have also been studied for photocatalysis, though rarely [27, 28]. A good alternative to single ion doping would be a combination doping of more than one rare earth ions into the matrix of ZnO and other semiconductor nanoparticles. Combination doping can have numerous high impact benefits over the conventional single ion doping. Presently very few literature precedents on combination doping are available [20, 29]. The curiosity of improvements in optoelectronic properties of semiconductors through multiple doping prompted us to extensively study the combination of La and Ce co-doping in the ZnO matrix. The main findings of the present research work can be summed-up to an optimized and much improved photocatalytic response and improved optical band gap of ZnO nanoparticles with respect to varied concentration of dopants used, shifting of absorption edge towards the visible region of the solar spectrum for more efficient utilization of the solar energy and better charge separation between photogenerated electrons and holes.

Various methods can be employed for the synthesis of rare earth ion doped ZnO nanoparticles like forced hydrolysis [30], pulsed laser deposition [31] and combustion method [32]. The chemical co-precipitation method used in this work for preparing La,Ce co-doped ZnO nanoparticles is low-cost, simple and does not involve any harmful chemicals or sophisticated machinery. ZnO nanoparticles with several dopant ion concentrations, i.e., Zn_{0.98}La_{0.01}Ce_{0.01}O, Zn_{0.96}La_{0.02}Ce_{0.02}O, Zn_{0.94}La_{0.03}Ce_{0.03}O and Zn_{0.92}La_{0.04}Ce_{0.04}O, were synthesized and studied for their structural, optical, photo-catalytic and photo-luminescence properties. The effect of incorporation of La,Ce co-dopant ions on microstructure, optical properties, photocatalytic and photoluminescence properties of ZnO, has been studied using XRD, SEM, UV-Visible spectrophotometry and photoluminescence, respectively. The degradation of Rhodamine B dye in presence of doped and undoped ZnO nanoparticles has been examined under UV light. A comparison of photocatalytic activity of doped and undoped nanoparticles shows that rare earth ion doping considerably improves the degradation of harmful dyes. The mechanism of dye degradation with La,Ce co-doped ZnO as photocatalyst is discussed in the present work.

Table 1. Standard conditions for synthesis of La, Ce co-doped ZnO nanoparticles ($Zn_{0.98}La_{0.01}Ce_{0.01}O$, $Zn_{0.96}La_{0.02}Ce_{0.02}O$, $Zn_{0.94}La_{0.03}Ce_{0.03}O$, $Zn_{0.92}La_{0.04}Ce_{0.04}O$)

Mole fraction (La and Ce)	Zinc acetate, M	Lanthanum acetate, M	Cerium acetate, M	Diethylamine, cc
0.00	0.50	0.00	0.00	0.50
0.01	0.50	0.005	0.005	0.50
0.02	0.50	0.010	0.010	0.50
0.03	0.50	0.015	0.015	0.50
0.04	0.50	0.020	0.020	0.50

EXPERIMENTAL

A simple wet chemical approach of co-precipitation was used for the synthesis of La,Ce co-doped ZnO nanoparticles ($Zn_{0.98}La_{0.01}Ce_{0.01}O$, $Zn_{0.96}La_{0.02}Ce_{0.02}O$, $Zn_{0.94}La_{0.03}Ce_{0.03}O$ and $Zn_{0.92}La_{0.04}Ce_{0.04}O$). La, Ce to Zn weight ratio was adjusted to maintain the mole fraction of the constituent ions in the nanoparticles. All the chemicals such as zinc acetate dihydrate [$Zn(COOCH_3)_2 \cdot 2(H_2O)$], lanthanum(III) acetate sesquihydrate [$La(CH_3COO)_3 \cdot 1.5H_2O$] and cerium(III) acetate tetrahydrate [$Ce(CH_3COO)_3 \cdot 4H_2O$], used as sources of dopants, respectively, were of high purity (Sigma Aldrich, 99% purity) and were used without further purification. Distilled water was used as solvent. Diethylamine was used as the reducing agent which in addition also acts a stabilizing agent. Undoped ZnO nanoparticles were synthesized by preparing 0.5 M zinc acetate solution in a beaker at 60°C. After that 5 mL of diethylamine was slowly added and reaction was carried on for another 30 min. Resulting solution was heated at 180°C followed by annealing at 500°C for 1 h. For La and Ce co-doped ZnO nanoparticles, 0.5 M zinc acetate solution was again prepared. Then solutions of lanthanum(III) acetate sesquihydrate and cerium(III) acetate tetrahydrate with different mole fractions varying from 0.00–0.04 with a step of 0.01 were added to it followed by drop wise addition of diethylamine. The resulting solution was stirred for additional 1 h. A set of samples of varying mole fractions of La and Ce from 0.00 to 0.04 were finally obtained in the form of clear homogenous solutions and were subjected to centrifuge in order to isolate the particles. Synthesized nanoparticle were cleaned with ethanol. The standard conditions and molarities used for synthesizing La,Ce co-doped ZnO nanoparticles are shown in Table 1.

The crystal structure of nanoparticles was determined using powder X-ray diffractometer with CuK_{α} target ($k = 1.54052 \text{ \AA}$) radiation over the range of 2θ from 10° – 90° with a step of 0.01° at room temperature. The surface morphologies of undoped and La,Ce co-doped ZnO nanoparticles were studied using SEM. The UV-Visible optical absorbance spectra of the undoped and La,Ce co-doped ZnO nanoparticles were carried out to study their optical properties using UV-visible spectrophotometer (Perkin Elmer, Lambda 35) in the wavelength range of 200–800 nm using quartz cuvettes at room temperature. The room temperature photoluminescence spectra of ZnO and La,Ce co-doped ZnO were recorded with a Horiba LabRam spectroscopy system with an excitation source of 325 nm and an accumulation time of 2 s.

Photocatalytic activity measurement. The photocatalytic degradation of doped and undoped nanoparticles was investigated in glass beaker (250 mL) under UV light using a triple jacketed photocatalytic reactor fitted with UV lamp of capacity 450 W.

The solution for photodegradation measurement was prepared by adding 0.1 g/L of $Zn_{0.98}La_{0.01}Ce_{0.01}O$, $Zn_{0.96}La_{0.02}Ce_{0.02}O$, $Zn_{0.94}La_{0.03}Ce_{0.03}O$ and $Zn_{0.92}La_{0.04}Ce_{0.04}O$ nanoparticles and 10 mg/L of Rhodamine B Dye in 30 mL of distilled water. Prior to illumination, the suspension was magnetically stirred continuously in the dark for half an hour to disperse the catalyst and establish an adsorption/desorption equilibrium. After that, the suspension was irradiated with UV light. During irradiation process, stirring was continued to keep the mixture in suspension. At given time intervals of irradiation, 3 mL of the dye solution was sampled and centrifugated immediately to remove the nanoparticles. The change in Rhodamine

B Dye concentration in each photodegraded solution was monitored by two sets of measurements. Firstly, the maximum absorbance of Rhodamine B Dye was measured at $\lambda_{\text{max}} = 650$ nm in an ultraviolet-visible spectrometer. Secondly, the total organic carbon was determined by CHN analyzer (ElementarVario EL III). Prior to the total organic carbon determination, the solution was filtered through a filter of 0.2 μm pore size to remove photocatalysts.

RESULTS AND DISCUSSION

Structural studies. Figure 1 shows the XRD pattern of undoped and La, Ce co-doped ($\text{Zn}_{0.98}\text{La}_{0.01}\text{Ce}_{0.01}\text{O}$, $\text{Zn}_{0.96}\text{La}_{0.02}\text{Ce}_{0.02}\text{O}$, $\text{Zn}_{0.94}\text{La}_{0.03}\text{Ce}_{0.03}\text{O}$ and $\text{Zn}_{0.92}\text{La}_{0.04}\text{Ce}_{0.04}\text{O}$) nanoparticles. All the diffraction peaks observed were indexed to hexagonal wurtzite phase of ZnO (JCPDS-98-002-6593). The diffraction pattern rules out presence of any secondary crystalline phases and impurities. All the XRD patterns show peak 011 with highest intensity indicating that all the samples are hexagonal with desirable orientation. There are no separate peaks of La, Ce or their oxides in the pattern indicating that La and Ce ions are well incorporated in the interstitial spaces of ZnO crystal structure without causing any change in it.

The ionic radii of La^{3+} and Ce^{3+} ions are 1.06 and 1.03 Å, respectively, and are quite large as compared to ionic radius of Zn^{2+} (0.72 Å). This mismatch leads to slight distortion in the lattice of ZnO. Furthermore, there is a shift towards higher angle in doped nanoparticles as compared to undoped ones, which confirms the smooth incorporation of La, Ce ions in ZnO lattice. The Debye Scherer's formula was used to calculate the average crystal size of samples using X-ray line broadening.

$$D = \frac{K\lambda}{\beta \cos \theta}, \quad (1)$$

where D is the average crystallite size, β is the line broadening measured at full width half maximum. K is a constant and its value is 1 in the current work [33]; λ represents wavelength of radiation (CuK_{α} , 1.54052 Å) and θ indicates the Bragg's angle. The grain size is found to get decreased with increase in doping concentration. The particle size of undoped ZnO nanoparticles is found to be 52 nm. The particle sizes of La,Ce co-doped ZnO nanoparticles viz. ($\text{Zn}_{0.98}\text{La}_{0.01}\text{Ce}_{0.01}\text{O}$,

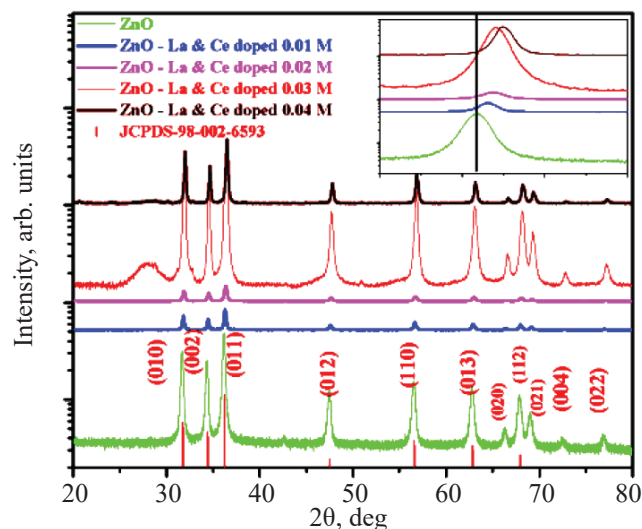


Fig. 1. (Color online) XRD pattern of undoped and La, Ce co-doped ZnO nanoparticles

$\text{Zn}_{0.96}\text{La}_{0.02}\text{Ce}_{0.02}\text{O}$, $\text{Zn}_{0.94}\text{La}_{0.03}\text{Ce}_{0.03}\text{O}$, and $\text{Zn}_{0.92}\text{La}_{0.04}\text{Ce}_{0.04}\text{O}$) were found to be 37, 25, 22, and 20 nm, respectively. The change in intensity of peaks as the doping concentration increases can be attributed to the change in grain morphology which can also be seen in the SEM images.

Morphological and compositional studies. The SEM images of undoped and La,Ce co-doped ZnO nanoparticles are shown in Fig. 2a–2e. The undoped ZnO nanoparticles shown in Fig. 2a are elongated rod type and bigger in size. $\text{Zn}_{0.98}\text{La}_{0.01}\text{Ce}_{0.01}\text{O}$ nanoparticles, as can be clearly seen from Fig. 2b, are smaller rod type in size. $\text{Zn}_{0.96}\text{La}_{0.02}\text{Ce}_{0.02}\text{O}$ nanoparticles as seen in Fig. 2c are spherical, but small in size. $\text{Zn}_{0.94}\text{La}_{0.03}\text{Ce}_{0.03}\text{O}$ nanoparticles (Fig. 2d) are spherical but smaller in size than $\text{Zn}_{0.96}\text{La}_{0.02}\text{Ce}_{0.02}\text{O}$ nanoparticles. Figure 2e shows $\text{Zn}_{0.92}\text{La}_{0.04}\text{Ce}_{0.04}\text{O}$ nanoparticles with smallest spherical particle size. The particles sizes as seen from images are seen to be consistent with the XRD data. The control in grain size as observed from different SEM images can be attributed to smaller ionic radii of La^{3+} and Ce^{3+} (1.06 and 1.0 Å, respectively) as compared to Zn^{2+} (0.72 Å). Hence, as the doping concentration increases the particle size decreases because of lattice strain caused by lattice mismatch of parent and dopant ions. It is evident from the SEM images that the dopant concentration influences the morphology of the nanoparticles. As the concentration of the dopant ions increases, the morphology changes from elongate rod to spherical shape which implies differential growth of

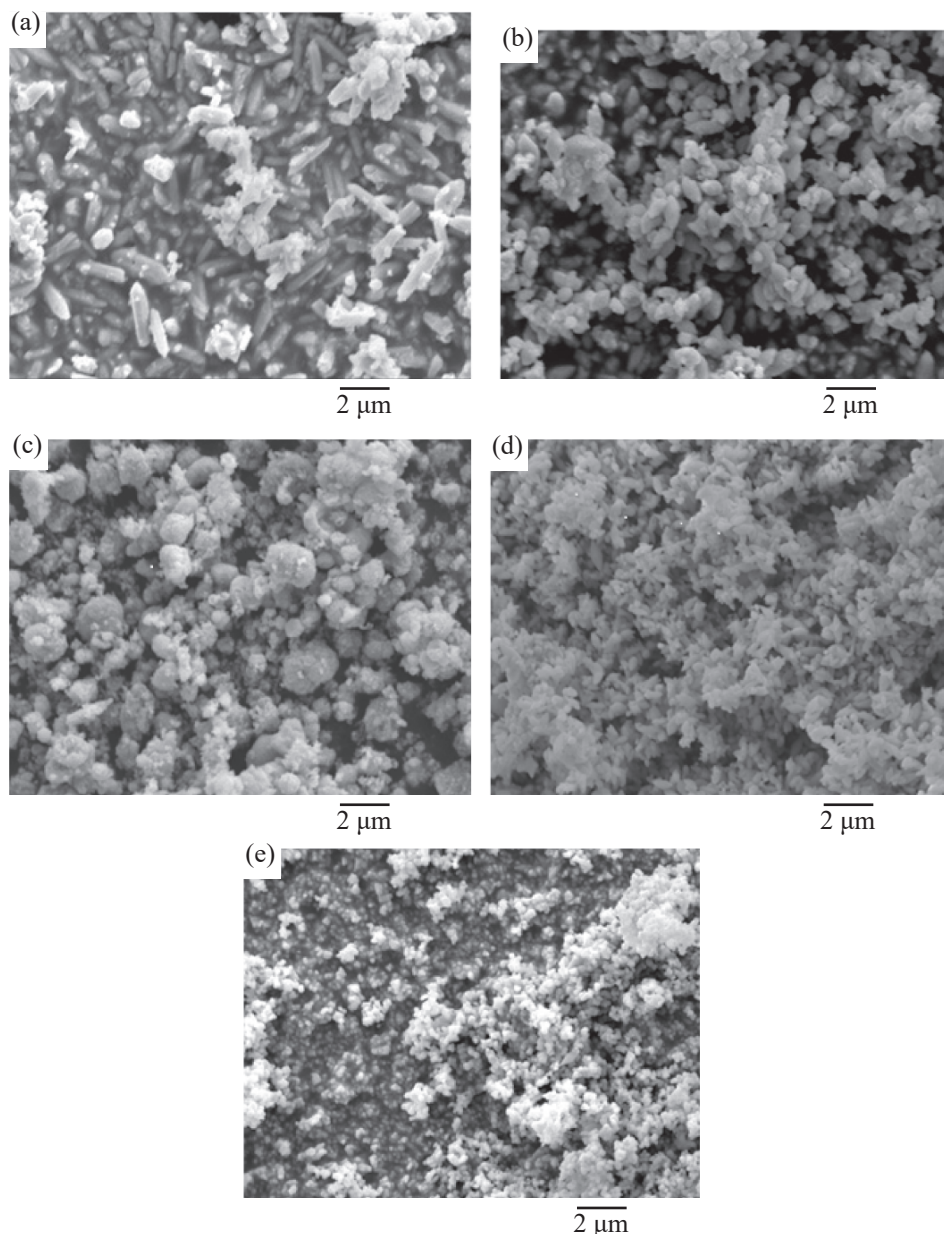


Fig. 2. SEM surface micrographs of undoped ZnO and La,Ce co-doped ZnO nanoparticles. (a) Undoped ZnO, (b) $\text{Zn}_{0.98}\text{La}_{0.01}\text{Ce}_{0.01}\text{O}$, (c) $\text{Zn}_{0.96}\text{La}_{0.02}\text{Ce}_{0.02}\text{O}$, (d) $\text{Zn}_{0.94}\text{La}_{0.03}\text{Ce}_{0.03}\text{O}$, (e) $\text{Zn}_{0.92}\text{La}_{0.04}\text{Ce}_{0.04}\text{O}$.

nanoparticles with increase in the lattice strain as the dopant concentration increases. This property of dopant concentration based morphology of ZnO nanoparticles can lead to interesting applications.

Optical studies. The study of optical properties is very important to evaluate the applications of nanomaterials. The band gap, additional energy levels and absorption edge of the undoped ZnO and La,Ce co-doped ZnO nanoparticles were evaluated using UV-Vis spectrometer in the range 200–800 nm. The

absorbance spectra are shown in Fig. 3. It was observed that $\text{Zn}_{0.92}\text{La}_{0.04}\text{Ce}_{0.04}\text{O}$ sample has highest optical absorbance because of smallest particles size. Figure 3 also revealed that the optical absorbance edge has shifted to visible range by co-doping of La and Ce ions into host ZnO matrix.

The band gap energy (E_g) of nanoparticles sample was calculated [34, 35] from the Eq. (2):

$$\alpha h\nu = A(h\nu - E_g)^{1/2}, \quad (2)$$

where $h\nu$ is the photon energy, A is a constant, and α is the optical absorption coefficient near the fundamental absorption edge. The absorption coefficients were calculated from the optical absorption spectra. The band gap of the sample was obtained by plotting of $(\alpha h\nu)^2$ vs. $h\nu$ in the high-absorption range followed by extrapolating the linear portion of the plots to $(\alpha h\nu)^2 = 0$, as shown in Figs. 4a–4e. The estimated energy gap for the undoped and La,Ce co-doped ZnO is shown in Table 2.

The band gap values of the undoped ZnO and La,Ce co-doped ZnO particles decreased from 3.097 to 2.354 eV. Red shift in the absorption edge and the narrowing of band gap can be attributed to the creation of oxygen vacancies upon doping and creation of additional energy levels in the bandgap of ZnO. This leads to increase in average atomic distance and decrease in bandgap. Oxygen vacancies assist the surface adsorbed oxygen to capture electron which in turn leads to generation of oxide radical. Hence oxygen vacancies lead to better photocatalysis.

Photoluminescence studies. Photoluminescence (PL) measurement is the best tool to investigate the optical properties and electronic structure of semiconducting materials. The information regarding the bandgap, generation and recombination of photo-induced charge carriers can be availed with the help of photoluminescence data [36, 37]. Photoluminescence also gives an insight into the surface oxygen states and defects of the semiconducting materials. Figure 5a shows PL spectrum of undoped and La,Ce co-doped ZnO nanoparticles ($\text{Zn}_{0.98}\text{La}_{0.01}\text{Ce}_{0.01}\text{O}$, $\text{Zn}_{0.96}\text{La}_{0.02}\text{Ce}_{0.02}\text{O}$, $\text{Zn}_{0.94}\text{La}_{0.03}\text{Ce}_{0.03}\text{O}$, $\text{Zn}_{0.92}\text{La}_{0.04}\text{Ce}_{0.04}\text{O}$, and $\text{Zn}_{0.90}\text{La}_{0.05}\text{Ce}_{0.05}\text{O}$). As can be clearly seen from Fig. 5a there are two prominent emission peaks in the PL spectrum of undoped ZnO nanoparticles, one in the UV region and another in the near IR region. The peak in the UV region is indicative of near band edge absorption via recombination, resulting from exciton-exciton collision process. The presence of emission peak in the near IR region can possibly be attributed to surface plasma resonance absorption [38, 39].

Rare earth doping has exciting consequences on the PL spectrum of ZnO. It can be seen that the peak in the UV region is significantly enhanced. Rare earth co-doping induces a red shift in the band gap of ZnO as can be seen from Fig. 5b. As the concentration of dopants

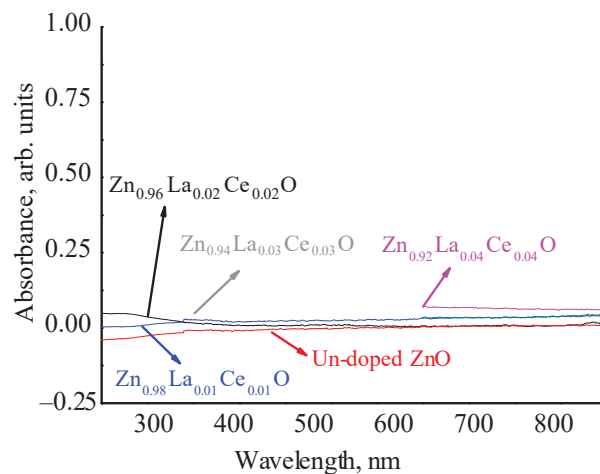


Fig. 3. Optical absorbance spectra of undoped ZnO and La,Ce co-doped ZnO nanoparticles. (a) Undoped ZnO, (b) $\text{Zn}_{0.98}\text{La}_{0.01}\text{Ce}_{0.01}\text{O}$, (c) $\text{Zn}_{0.96}\text{La}_{0.02}\text{Ce}_{0.02}\text{O}$, (d) $\text{Zn}_{0.94}\text{La}_{0.03}\text{Ce}_{0.03}\text{O}$, (e) $\text{Zn}_{0.92}\text{La}_{0.04}\text{Ce}_{0.04}\text{O}$ nanoparticles.

increases, the red shift is further enhanced for peaks in UV region shift further to higher wavelengths.

The possible explanation for red shift towards the visible range can be attributed to the formation of electronic states from rare earth dopants at the bottom edge of conduction band. The mechanism behind this can be explained with one of the following phenomenon:

(a) The dopant ions La^{3+} ($5d^16s^2$) and Ce^{3+} ($4f^15d^16s^2$) create a localized impurity state near lower edge of conduction band. This donor impurity band merges with the conduction band leading to a reduced band gap of ZnO. Similar phenomenon has been reported for Ce doped nitrides [40].

(b) Valence band and conduction band can be tailored by potential fluctuations caused by ionized impurities. This tailoring contributes to narrowing of band gap. The fluctuations lead to narrow optical transitions within

Table 2. Undoped and La,Ce co-doped ZnO nanoparticle and their corresponding bandgaps

Nanoparticle	Band gap energy, eV
Undoped ZnO	3.097
$\text{Zn}_{0.98}\text{La}_{0.01}\text{Ce}_{0.01}\text{O}$	2.872
$\text{Zn}_{0.96}\text{La}_{0.02}\text{Ce}_{0.02}\text{O}$	2.656
$\text{Zn}_{0.94}\text{La}_{0.03}\text{Ce}_{0.03}\text{O}$	2.368
$\text{Zn}_{0.92}\text{La}_{0.04}\text{Ce}_{0.04}\text{O}$	2.354

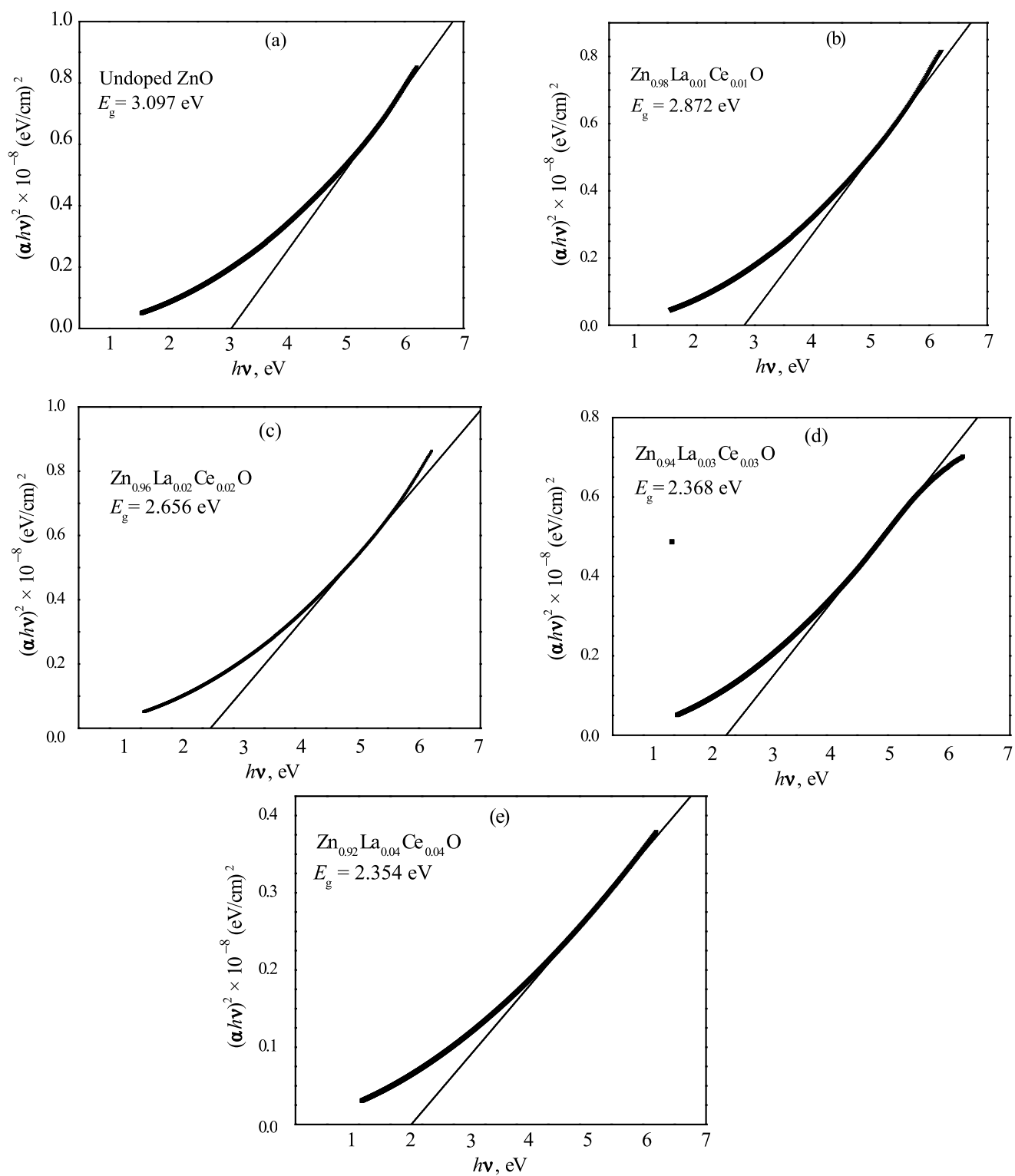


Fig. 4. The $(\alpha/h\nu)^2$ vs. $h\nu$ diagram for the optical energy band gap determination of undoped ZnO and La,Ce co-doped ZnO nanoparticles. (a) Undoped ZnO, (b) $\text{Zn}_{0.98}\text{La}_{0.01}\text{Ce}_{0.01}\text{O}$, (c) $\text{Zn}_{0.96}\text{La}_{0.02}\text{Ce}_{0.02}\text{O}$, (d) $\text{Zn}_{0.94}\text{La}_{0.03}\text{Ce}_{0.03}\text{O}$, (e) $\text{Zn}_{0.94}\text{La}_{0.04}\text{Ce}_{0.04}\text{O}$.

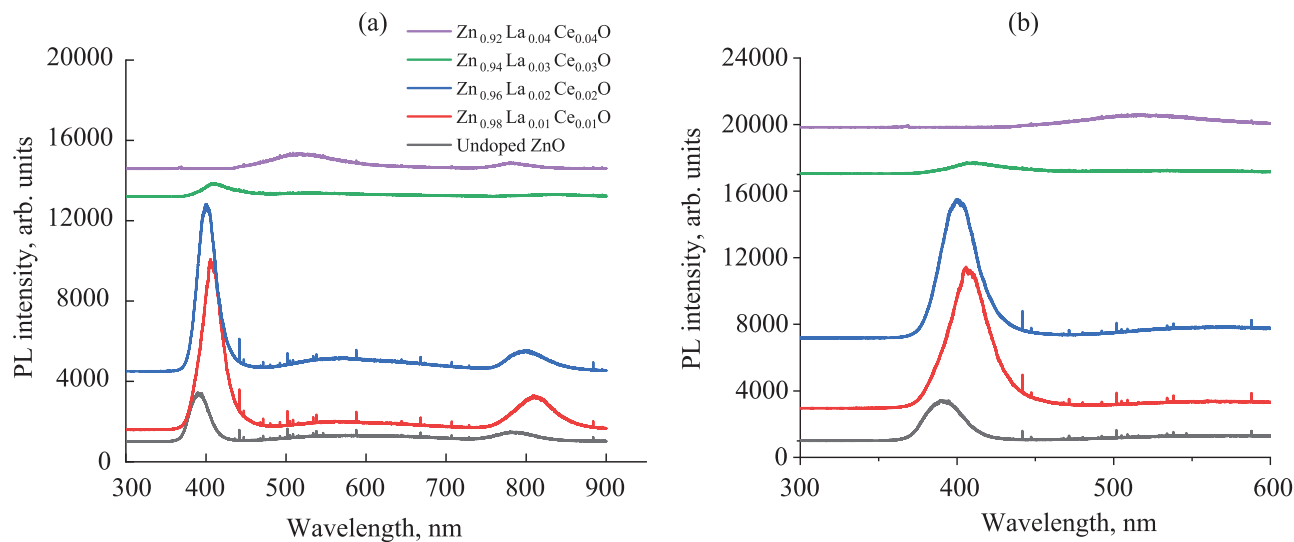
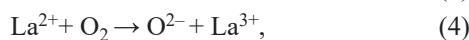
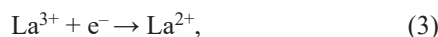


Fig. 5. (Color online) (a) Room temperature PL spectrum of undoped and La,Ce co-doped ZnO nanoparticles. (b) Expanded UV region of the spectrum showing red shift in wavelength with increase in concentration of dopants.

the spin orbital levels. This causes an absorption edge transition from $2p$ orbital of oxygen to $5d$ orbital of La and $4f$ orbital of Ce in case of La,Ce co-doped ZnO compared to transition from $3d$ orbital of Zn in case of undoped ZnO [20].

(c) The Pauli's electronegativities of La (1.10) and Ce (1.12) are much less as compared to Zn (1.65). The isoelectronic traps formed by La^{3+} and Ce^{4+} can bind a hole and an electron (e^-) through coulombic interaction, giving rise to an acceptor bound excitation pair [41]. The molecular oxygen, adsorbed on the surface of nanoparticles, can result in possible trapping of co-dopants. This can be explained with following reactions.



This charge transfer between the valence band or conduction band of ZnO and $4f$ and $5d$ levels of Ce and La, respectively, can be the reason for red shift or narrowing of band gap in La,Ce co-doped nanoparticles. This is based on the fact that electron-electron and electron-impurity interaction lead to upward shift of valence band, lowering of conduction band and hence overall narrowing of band gap [42]. It can also be observed from Fig. 5a that the intensity of photoluminescence decreases with higher doping concentration. With

increase in doping concentration, it is expected that the surface bound states act as defect states resulting in non radiative relaxation. The photoluminescence intensity depends on distance between these states and their center to center interaction. The energy can migrate in a non-radiative manner if there is spectral overlap of wave functions from these states which ultimately leads to decreased intensity [43].

Photocatalytic activities. Photocatalytic activities of undoped ZnO and La,Ce co-doped ZnO nanoparticles were studied using Rhodamine B dye under UV irradiation. The degradation of Rhodamine B dye with undoped and doped ZnO nanoparticles as catalyst under UV irradiation is shown in Figs. 6a–6e at different reaction times (0–80 min).

Degradation is indicated by decrease in absorbance with increase in reaction time. It can be clearly seen from Figs. 6a–6e that using La,Ce co-doped ZnO nanoparticles as catalyst, the dye shows a considerable degradation as compared to undoped ZnO nanoparticles.

Figure 7a shows the comparative photodegradation of Rhodamine B dye with reference to initial concentration of undoped ZnO and La,Ce co-doped ZnO nanoparticles. The degradation is seen to be most efficient and fast with $\text{Zn}_{0.98}\text{La}_{0.04}\text{Ce}_{0.04}\text{O}$ nanoparticles as catalyst.

Figure 7b shows the reaction kinetics of photodegradation of Rhodamine B dye with undoped and doped ZnO nanoparticles during different reaction times

(0–80 min). Slope of Fig. 7b gives us the value of rate constant (K) for photochemical reactions. A simplified pseudo first order kinetic equation for photo degradation can be written as [44]

$$\ln(C_t/C_0) = Kt, \quad (7)$$

where C_0 is the initial concentration of the dye, C_t is the concentration of dye in selected interval after irradiation with UV light. K is the first order rate constant

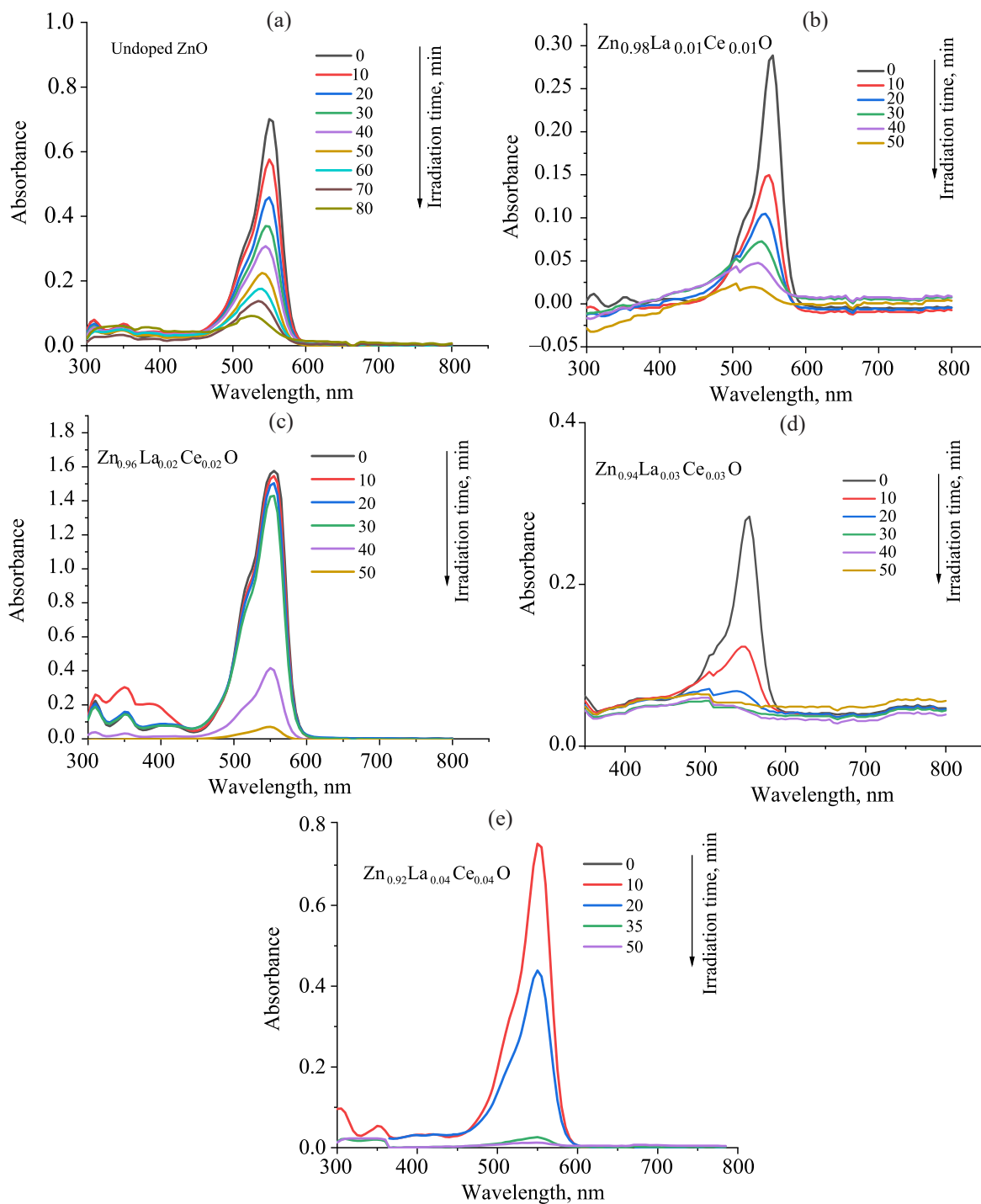


Fig. 6. (Color online) UV-Vis Absorbance spectral changes of Rhodamine B dye solution during photocatalytic degradation with undoped and La,Ce co-doped ZnO nanoparticles as catalyst under UV irradiation at different time intervals. (a) Undoped ZnO nanoparticles, (b) $Zn_{0.98}La_{0.01}Ce_{0.01}O$, (c) $Zn_{0.96}La_{0.02}Ce_{0.02}O$, (d) $Zn_{0.94}La_{0.03}Ce_{0.03}O$, (e) $Zn_{0.92}La_{0.04}Ce_{0.04}O$.

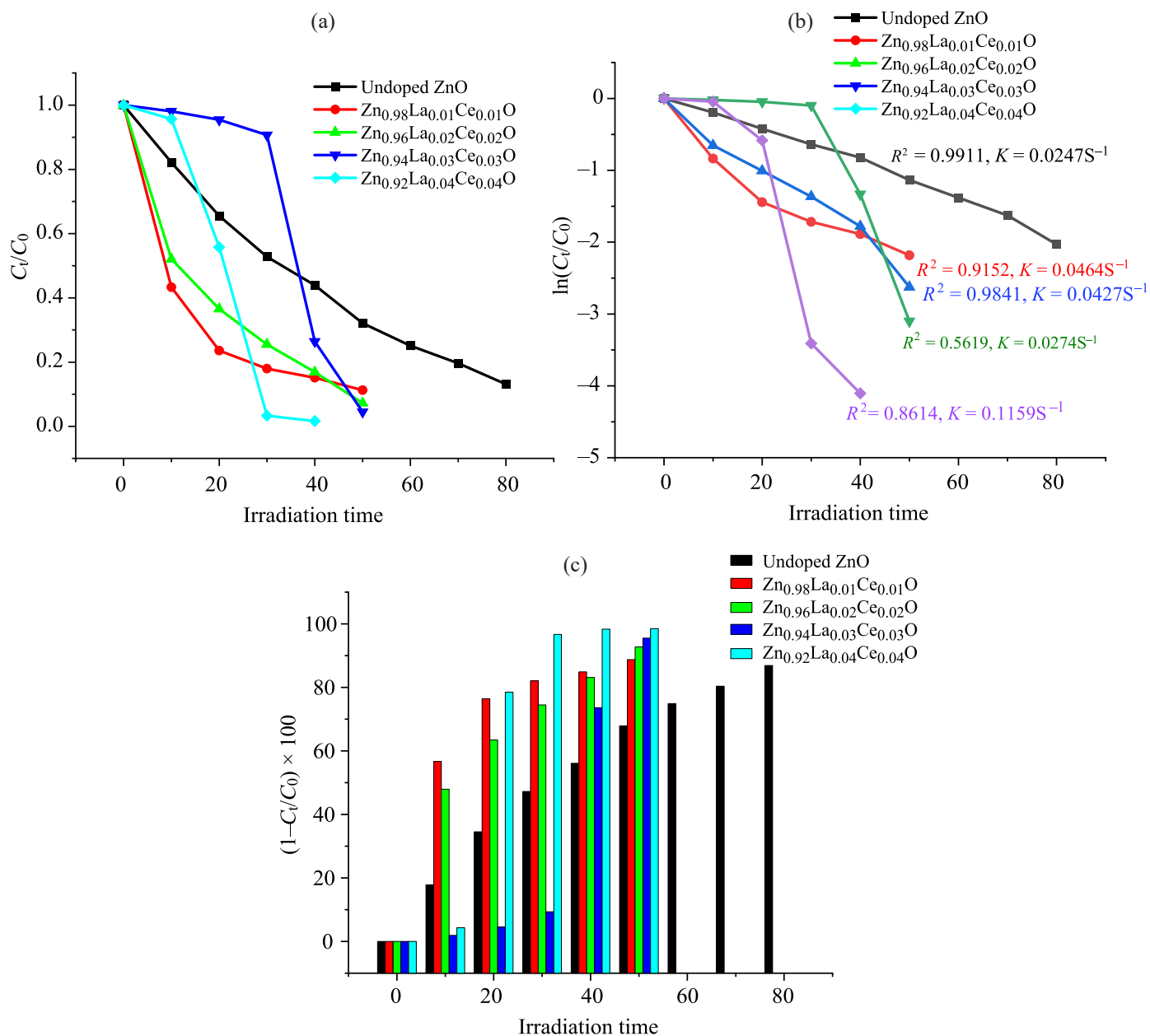


Fig. 7. (Color online) (a) Photocatalytic degradation of Rhodamine B dye solution with undoped ZnO and La,Ce co-doped ZnO nanoparticles. (b) Reaction kinetics of photocatalytic degradation with undoped ZnO nanoparticles and La,Ce co-doped ZnO nanoparticles under UV irradiation at different time intervals. (c) Photocatalytic degradation percentage of Rhodamine B dye solution with undoped ZnO and La,Ce co-doped ZnO nanoparticles under UV irradiation at different time intervals.

and t is the irradiation time. The value of K is found by linear fitting of slopes and is found to be $0.0247 S^{-1}$ for undoped ZnO nanoparticles, and 0.0464 , 0.0427 , 0.0274 , and $0.1159 S^{-1}$ for $Zn_{0.98}La_{0.01}Ce_{0.01}O$, $Zn_{0.96}La_{0.02}Ce_{0.02}O$, $Zn_{0.94}La_{0.03}Ce_{0.03}O$ and $Zn_{0.92}La_{0.04}Ce_{0.04}O$, respectively.

This result is in coherence with degradation of Rhodamine B dye with other catalysts also. The $Zn_{0.98}La_{0.04}Ce_{0.04}O$ nanoparticles show the highest rate constant value.

Figure 7c shows the photocatalytic degradation percentage with undoped and La,Ce co-doped ZnO nanoparticles at different reaction times under

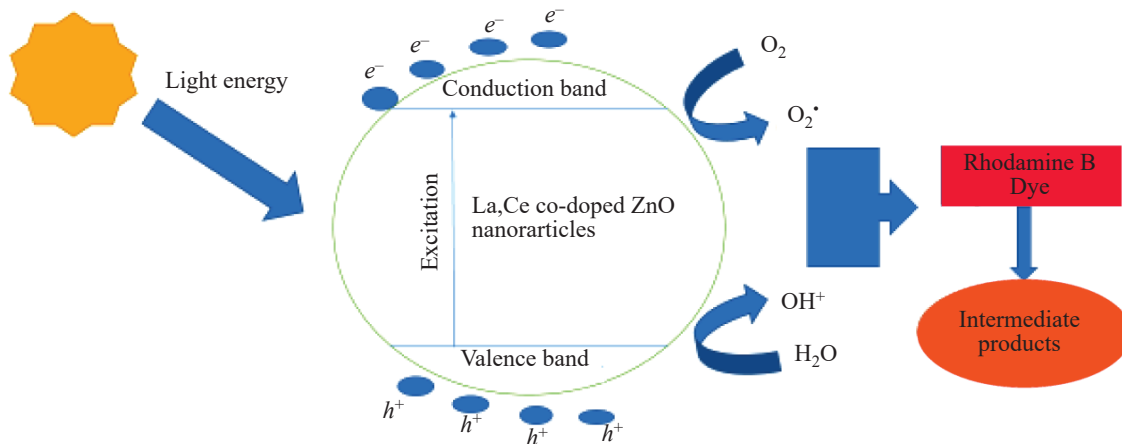


Fig. 8. (Color online) Schematic diagram of mechanism of degradation of dye with La,Ce co-doped ZnO nanoparticles as catalyst.

UV irradiation. The formula for calculating the degradation (D , %) efficiency is given below.

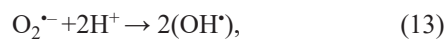
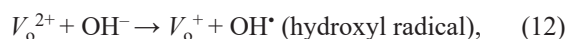
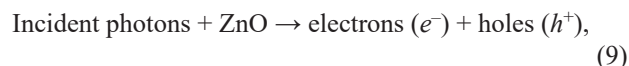
$$D = \left(1 - \frac{C_t}{C_0}\right) \times 100, \quad (8)$$

where C_t represents the concentration of dye after UV irradiation, C_0 represents concentration of dye before irradiation. Figure 7c reveals that the efficiency of degradation is highest with $\text{Zn}_{0.98}\text{La}_{0.04}\text{Ce}_{0.04}\text{O}$, i.e. 98%.

MECHANISM OF DEGRADATION

Enhancement of photocatalytic activity with lanthanum and cerium co-doping can be explained the basis of dye degradation mechanism as follows. The semiconductor nano-photocatalyst ZnO is excited with photons of ultraviolet region having energy ($h\nu$) greater than its bandgap. Excitation generates electron-hole pairs on the surface of semiconductor (Eq. 9). The photo-generated electrons are trapped by the O_2 adsorbed on the surface of nanoparticles, the step which determines the rate of overall photocatalytic reaction. The $4f$ configuration of co-dopants La,Ce plays the pivotal role in generation, charge transfer and prevention of electron-hole recombination. La^{4+} and Ce^{4+} act as scavengers for the electrons from conduction band. In addition, La^{4+} and Ce^{4+} are stronger Lewis acids as compared to O_2 and can efficiently trap electrons adsorbed by O_2 . Hence the co-dopants trap electrons, which by oxidative process get transferred to surface adsorbed oxygen and produce super oxide ($\text{O}_2^{\bullet-}$) (Eq. 10). Also the photo-generated electrons and holes can easily recombine and dissipate the energy as heat in absence of a defect state. However, defect states prevent

the recombination of electrons and holes and thus heat dissipation. The present work reports the enhancement of separation between the electron-hole energy levels created by single oxygen vacancy (V_o^+) in the bandgap of ZnO. Oxygen acts as an electron donor and forms charged oxygen vacancy which acts as trap for holes, thereby preventing the recombination of electrons and holes (Eq. 11). Charged oxygen vacancy on reaction with hydroxyl ion (OH^-) forms hydroxyl radical (OH^\bullet) (Eq. 12), which is a strong oxidant like the superoxide. Hydroxyl radical (OH^\bullet) can also be formed by reaction of superoxide anion with protons (H^+) (Eq. 13). These hydroxyl radicals are the main oxidants responsible for degradation of Rhodamine B (RB) to photodegraded intermediates which are ultimately converted to Carbon dioxide (CO_2) and water (H_2O) (Eq. 14). The following reactions depict the mechanism of dye degradation:



In addition to trapping the holes, oxygen vacancies also help in adsorbing oxygen which greatly enhances the photocatalysis [45]. This mechanism is illustrated with the help of schematic diagram in Fig. 8. As can be inferred from the above discussion, efficiency of photocatalysts depends on various factors such as

number of charge carriers at the surface of photocatalyst and electron-hole recombination rate which in turn depends on the bandgap. The present communication reports the enhancement in photocatalytic efficiencies of La and Ce co-doped ZnO nanoparticles compared to undoped ZnO photocatalysts. $Zn_{0.92}La_{0.04}Ce_{0.04}$ exhibited the best photocatalytic activity. The improved photocatalytic ability of La and Ce co-doped ZnO nanoparticles can be ascribed to the loading of dopant ions on the surface of host particles and availability of oxygen vacancies which accelerates the transport of charge carriers (electrons) to the adsorbed oxygen molecules. Further, more number of charge carriers are available on the surface due to decreased size and increased surface area as is clear from the SEM analysis. The photoluminescence study of La and Ce co-doped ZnO revealed the shift of absorption edge towards the visible portion of solar spectrum and consequent bandgap narrowing. This eventually leads to better utilization of solar energy and hence more efficient photocatalysis (Fig. 5). Further, photoluminescence study reveals incorporation of additional energy levels in the bandgap of ZnO due to La,Ce co-doping which delays the recombination of charge carriers that leads to enhanced degradation of Rhodamine B dye. The red shift in the absorption wavelength and the narrowing of bandgap is also confirmed by the UV-Vis analysis of undoped and La,Ce co-doped ZnO nanoparticles.

CONCLUSIONS

Undoped and La,Ce co-doped ZnO nanoparticles were successfully synthesized using co-precipitation technique. XRD analysis confirmed the formation of above mentioned nanoparticles in hexagonal wurtzite phase without any oxides or impurities. UV-Visible spectrophotometry revealed that co-doping of ZnO nanoparticles with La and Ce ions increases the visible light absorbance ability as compared to undoped ZnO nanoparticles. Morphology studies of the nanoparticles were carried out through scanning electron microscopy (SEM). Photoluminescence studies were performed to understand the physical band gap tailoring in La,Ce co-doped ZnO nanoparticles. The red shift in emission band towards visible region due to strong interactions between $4f-4f$, $5d-4f$, and $5d-5d$ orbitals may improve the potential of La,Ce co-doped ZnO as materials for light activated devices. The investigation

of photocatalytic activity reveals that rare earth doping of La and Ce into ZnO matrix enhances its degradation efficiency because of the $4d$ and $5f$ electronic structure. The delay in recombination in La,Ce co-doped samples due to additional defect levels in the bandgap and increased surface oxygen vacancies also contributes towards making the La,Ce co-doped samples much better and efficient photocatalysts.

CONFLICT OF INTERESTS

The authors declare that they have no conflicts of interest requiring disclosure in this article.

REFERENCES

1. Xu, H., Wang, W., and Zhu, W., *J. Phys. Chem.*, 2006, vol. 110, pp. 13829–13834. <https://doi.org/10.1021/jp061934y>
2. El-Sayed, M.A., *Acc. Chem. Res.*, 2001, vol. 34, pp. 257–264. <https://doi.org/10.1021/ar960016n>
3. Abdullah, M., Morimoto, T., and Okuyama, K., *Adv. Funct. Mater.*, 2003, vol. 13, pp. 800–804. <https://doi.org/10.1002/adfm.200304330>
4. Karnan, T., Arul, S., and Kumar, S.S., *J. Mol. Struct.*, 2016, vol. 1125, pp. 358–365. <https://doi.org/10.1016/j.molstruc.2016.07.029>
5. VanDijken, A., Meulenkamp, E.A., Vanmaekelbergh, D., and Meijerink, A., *J. Luminesc.*, 2000, vol. 90, pp. 123–128. [https://doi.org/10.1016/S0022-2313\(99\)00599-2](https://doi.org/10.1016/S0022-2313(99)00599-2)
6. Volbers, N., Zhou, H., Knies, C., Pfisterer, D., Sann, J., Hofmann, D.M., and Meyer, B.K., *Appl. Phys. A*, 2007, vol. 88, pp. 153–155. <https://doi.org/10.1007/s00339-007-3960-6>
7. Rau, U., and Schmidt, M., *Thin Solid Films*, 2001, vol. 387, pp. 141–146. [https://doi.org/10.1016/S0040-6090\(00\)01737-5](https://doi.org/10.1016/S0040-6090(00)01737-5)
8. Soki, T., Hatanaka, Y., and Look, D., *Appl. Phys. Lett.*, 2003, vol. 76, pp. 3257–3259. <https://doi.org/10.1063/1.126599>
9. Tang, Z., Wong, G., Yu, P., Kawasaki, M., Ohtomo, A., and Koinuma, H., *Appl. Phys. Lett.*, 1998, vol. 72, pp. 3270–3277. <https://doi.org/10.1063/1.121620>
10. Dindar, B. and Icli, S. *J. Photochem. Photobiol. A*, 2001, vol. 140, pp. 263–268.

- [https://doi.org/10.1016/S1010-6030\(01\)00414-2](https://doi.org/10.1016/S1010-6030(01)00414-2)
11. Hoffmann, M.R., Martin, S.T., Choi, W.Y., and Bahnemann, D.W., *Chem. Rev.*, 1995, vol. 95, pp. 69–96. <https://doi.org/10.1021/cr00033a004>
 12. Asahi, R., Morikawa, T., Ohwaki, T., Aoki, K., and Taga, Y., *Science*, 2001, vol. 293, pp. 269–271. <https://doi.org/10.1126/science.1061051>
 13. Qiu, R.L., Zhang, D.D., Yueqi, M., Lin, S., Brewer, E., Huang, X.F., et al., *J. Hazard.Mater.*, 2008, vol. 156, pp. 80–85. <https://doi.org/10.1016/j.jhazmat.2007.11.114>
 14. Kumaran, N.N. and Muraleedharan, K., *J.Water.Proc. Eng.*, 2017, vol. 17, pp. 264–270. <https://doi.org/10.1016/j.jwpe.2017.04.014>
 15. Nair, M., Luo, Z.H., and Heller, A., *Ind. Eng. Chem. Res.*, 1993, vol. 32, pp. 2318–2323. <https://doi.org/10.1021/ie00022a015>
 16. Boer, K.W., *Survey of Semiconductor Physics*, Van Nostrand Reinhold: New York, 1990, pp. 249.
 17. Linsebigler, A.L., Lu, G.Q., and Yates, Jr.J.T., *Chem. Rev.*, 1995, vol. 95, pp. 735–758. <https://doi.org/10.1021/cr00035a013>
 18. Romero, M., Blanco, J., Sanchez, B., Vidal, A., Malato, S., Cardona, A., et al., *Sol. Energy*, 1999, vol. 66, pp. 169–182. [https://doi.org/10.1016/S0038-092X\(98\)00120-0](https://doi.org/10.1016/S0038-092X(98)00120-0)
 19. Guan, K.S. and Yin, Y.S., *Mater. Chem. Phys.*, 2015, vol. 92, no. 19, pp. 16905–16912. <https://doi.org/10.1021/acs.jpcc.5b02485>
 20. Iqbal, J., Liu, X., Zhu, H., Wua, Z.B., Zhang, Y., Yu, D., and Yu, R., *Acta Mater.*, 2009, vol. 57, pp. 4790–4796. <https://doi.org/10.1016/j.actamat.2009.06.056>
 21. Pascariu, P., Homocianu, M., Cojocaru, C., Samoila, P., Airinei, A., and Sucheana, M., *Appl. Surf. Sci.*, 2019, vol. 476, pp. 16–27. <https://doi.org/10.1016/j.apsusc.2019.01.077>
 22. Romero, M., Blanco, J., Sanchez, B., Vidal, A., Malato, S., Cardona, A.I., et al., *Sol. Energy*, 1999, vol. 66, pp. 169–182. [https://doi.org/10.1016/S0038-092X\(98\)00120-0](https://doi.org/10.1016/S0038-092X(98)00120-0)
 23. Guan, K.S. and Yin, Y.S., *Mater Chem. Phys.*, 2005, vol. 92, pp. 10–15. <https://doi.org/10.1016/j.matchemphys.2004.01.044>
 24. Wanger, C.D., Riggs, W.M., Davis, L.E., and Moulder, F.J., *Handbook of XPS*, Eden Prairie MN: Perkin Elmer Corporation., 1979. <https://doi.org/10.1002/sia.740030412>
 25. Arguello, C.A., Rousseau, D.L., and Porto, S.P.S., *Phys. Rev.*, 1969, vol. 181, pp. 1351–1363. <https://doi.org/10.1103/PhysRev.181.1351>
 26. Zhang, W.F., Zhang, M.S., Yin, Z., and Chen, Q., *Appl. Phys. B*, 2000, vol. 70, pp. 261–265. <https://doi.org/10.1007/s003400050043>
 27. Khatamian, M., Khandar, A.A., Divband, B., Haghighi, M., and Ebrahimiasl, S., *J. Mol. Catal. A. Chem.*, 2012, vol. 365, pp. 120–127. <https://doi.org/10.1016/j.molcata.2012.08.018>
 28. Sin, J.C., Lam, S.M., Lee, K.T., and Mohamed, A.R., *J. Colloid Interf. Sci.*, 2013, vol. 401, pp. 40–49. <https://doi.org/10.1016/j.jcis.2013.03.043>
 29. Rahman, A. and Jayaganthan, R., *Trans. Indian Inst. Met.*, 2016, vol. 70, pp. 1063–1074. <https://doi.org/10.1007/s12666-016-0897-5>
 30. Li, X.Z., Li, F.B., Yang, C.L., and Ge, W.K., *J. Photochem. Photobiol. A*, 2001, vol. 141, pp. 209–217. [https://doi.org/10.1016/S1010-6030\(01\)00446-4](https://doi.org/10.1016/S1010-6030(01)00446-4)
 31. Jing, L.Q., Sun, X.J., Cai, W.M., Xu, Z.L., Du, Y.G., and Fu, H.G., *J. Phys. Chem. Solid.*, 2003, vol. 64, pp. 615–623. [https://doi.org/10.1016/S0022-3697\(02\)00362-1](https://doi.org/10.1016/S0022-3697(02)00362-1)
 32. Yamashita, H., Ichihashi, Y., Zhang, S.G., Matsumurab, Y., Soumab, Y., Tatsumic, T., et.al., *Appl. Surf. Sci.*, 1997, vol. 121, pp. 305–311. [https://doi.org/10.1016/S0169-4332\(97\)00311-5](https://doi.org/10.1016/S0169-4332(97)00311-5)
 33. Zou, D., Yan, D., Xiao, L., and Dong, Y., *Surf. Coat. Technol.*, 2008, vol. 202, pp. 1928–1934. <https://doi.org/10.1016/j.surfcoat.2007.08.022>
 34. Elilarassi, R. and Chandrasekaran, G., *J. Mater. Sci. Mater. Electron*, 2010, vol. 21, pp. 1168–1173. <https://doi.org/10.1007/s10854-009-0041-y>
 35. Yayapao, O., Thongtem, T., Phuruangrat, A., and Thongtem, S., *J. Alloy. Compnd.*, 2013, vol. 576, pp. 72–79. <https://doi.org/10.1016/j.jallcom.2013.04.133>
 36. Anbuvarannan, M., Ramesh, M., Viruthagiri, S.N., and Kannadasan, N., *Mater. Sci. Semicond. Process*, 2015, vol. 39, pp. 621–628. <https://doi.org/10.1016/j.mssp.2015.06.005>
 37. Zhang, W.F., Zhang, M.S., Yin, Z., and Chen, Q., *Appl. Phys.*, 2000, vol. 70, pp. 261–265. <https://doi.org/10.1007/s003400050043>

38. Zeng, J.H., Yu, Y.L., Wang, Y.F., and Lou, T., *J. Acta Mater.*, 2009, vol. 57, pp. 1813–1820.
<https://doi.org/10.1016/j.actamat.2008.12.021>
39. Iqbal, J., Wang, B., Liu, X.F., Yu, D.P., He, B., and Yu, R.H., *New J. Phys.*, 2009, vol. 11, pp. 63009–63014.
<https://doi.org/10.1088/1367-2630/11/6/063009>
40. Majid, A. and Ali, A., *J. Phys. D. Appl. Phys.*, 2009, vol. 42, pp. 45412–45416.
<https://doi.org/10.1088/0022-3727/42/4/045412>
41. Bhatia, S. and Verma, N., *Mater. Res. Bull.*, 2017, vol. 95, pp. 468–476.
<https://doi.org/10.1016/j.materresbull.2017.08.019>
42. Berggren, K.F. and Sernelius, B.E., *Phys. Rev.*, 1971, vol. 24, pp. 1971–1986.
<https://doi.org/10.1103/PhysRevB.24.1971>
43. George, A., Sharma, S.K., Chawla, S., Malik, M.M., and Qureshi, M.S., *J. Alloys Compd.*, 2011, vol. 509, pp. 5942–5946.
<https://doi.org/10.1016/j.jallcom.2011.03.017>
44. Wang, S., Bai, L., and Ao, X., *RSC Adv.*, 2018, vol. 8, pp. 36745–36753.
<https://doi.org/10.1039/C8RA06778C>
45. Chang, C.J., Lin, C.Y., and Hsu, M.H., *J. Taiwan. Inst. Chem. Eng.*, 2014, vol. 45, pp. 1954–1963.
<https://doi.org/10.1016/j.jtice.2014.03.008>